

Article

Sensitivity Analysis of Event-Specific Calibration Data and Its Application to Modeling of Subaerial Storm Erosion under Complex Bathymetry

Hyeok Jin ^{1,2} , Kideok Do ^{1,*} , Inho Kim ³ and Sungyeol Chang ⁴

¹ Department of Convergence Study on the Ocean Science and Technology, Korea Maritime & Ocean University, Busan 49112, Korea

² Department of Marine Forecast, Geosystem Research Inc., Gunpo-si 15807, Korea

³ Department of Earth and Environmental Engineering, Kangwon National University, Chuncheon-si 25913, Korea

⁴ Haeyeon Engineering and Consultants Corporation, Gangneung-si 25623, Korea

* Correspondence: kddo@kmou.ac.kr; Tel.: +82-51-410-5248

Abstract: Key parameters in a process-based model depicting the morphological changes during storm events should be adjusted to simulate the hydro- and morphodynamics, leading to site-, profile-, and event-specific calibration. Although area models eliminate variability in calibrated parameters along with each profile in complex bathymetry, the amount of influence datasets with different wave conditions have on model performance is still unclear in an area model in a given parameter space. This study collected hydrodynamic and bathymetric field data over four different storm conditions (two single and two cluster storms) at Maengbang Beach, South Korea. The numerical model XBeach was adopted using four storm datasets with four key parameters to examine the influence of event-specific calibration data on subaerial storm erosion. When using clustered storm data, a relatively limited number of parameter combinations showed higher model sensitivity to different parameter sets as opposed to single storm data with the same parameter sets. Model sensitivity to different storm events was correlated with cumulative storm power and resultant erosion volume in comparison with other features in the datasets. The results are expected to guide the selection of an event-specific dataset with various morphological and hydrodynamic factors in an area model under complex bathymetry.

Keywords: coastal erosion; XBeach; model calibration; storm cluster; crescentic bar; megacusps



Citation: Jin, H.; Do, K.; Kim, I.; Chang, S. Sensitivity Analysis of Event-Specific Calibration Data and Its Application to Modeling of Subaerial Storm Erosion under Complex Bathymetry. *J. Mar. Sci. Eng.* **2022**, *10*, 1389. <https://doi.org/10.3390/jmse10101389>

Academic Editor: Edward J. Anthony

Received: 12 August 2022

Accepted: 23 September 2022

Published: 28 September 2022

Publisher's Note: MDPI stays neutral with regard to jurisdictional claims in published maps and institutional affiliations.



Copyright: © 2022 by the authors. Licensee MDPI, Basel, Switzerland. This article is an open access article distributed under the terms and conditions of the Creative Commons Attribution (CC BY) license (<https://creativecommons.org/licenses/by/4.0/>).

1. Introduction

The erosion of sandy beaches stems from sediment supply limitations, human intervention, extreme storms, and sea-level rise due to climate change [1]. Storm-induced erosion can lead to intense short-term damage in coastal regions, highlighting the need for hazard mitigation and coastal erosion early warning systems [2] based on several numerical models (e.g., CSHORE [3], SBEACH [4], and XBeach [5]). Each model has various semi-empirical parameters to simulate the appropriate hydro- and morphodynamics in a specific area of interest. However, these parameters are event-, site-, and profile-specific in model calibration because the beach response to storm events varies with the complexity of the sandy beach environment. Profile-specific calibration [6–8] is used to select a suitable parameter set for a specific profile in one-dimensional profile models. The profile model is favorable in areas with alongshore uniformity, which assumes no distinct variability alongshore because it can produce various simulation cases at relatively low computational costs. Previous works by Simmons et al., 2017 [6] and 2019 [7] reported the improvement of predictive skills by profile-specific calibration with rigorous calibration through Monte Carlo sampling (i.e., the generalized likelihood uncertainty estimation (GLUE) method [6]). Elsayed et al., 2017 [8] pointed out the correlation between optimum parameters of wave

shape and initial seaward slopes. Therefore, the performance of each profile along the shore can be improved through profile-specific calibration of the beach/dune erosion. However, their alongshore uniform assumption has limitations in complex bathymetry, where rhythmic sandbars and shoreline patterns or hard structures for coastal maintenance projects are dominant. For instance, crescentic sandbars that are predominantly found in microtidal sandy beaches on relatively gentle slopes (less than 1:20) [9] have been associated with shoreline undulations (megacusps) [10–12]. Many factors, such as wave direction, wave height, water level, and initial variability in bathymetry, affect each factor complexly, constantly changing erosive and accretive locations. In addition, the shoreline response to coastal protection structures varies with wave conditions and features of the structures [13,14]. In such bathymetries, profile-specific calibration is highly variable, which leads to the need for continuous calibration processes at a fixed profile in response to changing conditions. Therefore, area models, especially the short-wave-averaged but infragravity-wave-resolving model XBeach (surfbeat mode, hereafter called “XBBSB”), should be employed to produce reliable results from such complex interactions between hydro- and morphodynamics without requiring extensive repetitive calibration. The area model in the XBBSB is irrelevant to profile-specific calibration and shows better model performance on the observed alongshore variability with calibrated parameters [15,16]. Although it incurs a higher computational cost than the profile model, covering alongshore variability with a parameter set saves time for adopting optimum parameter values along with varying profiles.

XBBSB was originally intended for applications with high wave energy for short durations on relatively gentle beach-face slopes (i.e., storm erosion on dissipative sandy beaches). This indicates that XBBSB with default settings is preferable to these conditions and may require event-specific calibration for different beach states [17–20]. In addition, storm clusters consisting of relatively small, isolated storm events can generate more significant erosion than a single large storm [21,22], which may cause different model sensitivities in the calibration process depending on the storm events. Thus, morphodynamic modelers cannot expect that the optimum parameter set already calibrated from single storm data can be applied to different storm events, even at the same site [23]. Furthermore, the degree to which the model performance depends on different incident wave conditions in the area model at a given parameter space remains unclear. Simmons et al., 2019 [7] suggested that the characteristics of storm events had less variability in selecting optimum parameters; thus, datasets covering spatial variation may be more important in terms of model calibration. However, Rafati et al., 2021 [20] showed a correlation between the optimum parameters and incident wave conditions, although all initial profiles differed. Several studies [11,24,25] simulated storm morphological changes under complex bathymetry where an area model is required but did not elucidate the model sensitivity to various incident wave events.

The objective of this study was to examine the influence of event-specific calibration data (single storm events and storm clusters) on the modeling of subaerial storm erosion under complex bathymetry. A complex process-based model (XBeach2D, area model) was employed for detailed analysis and quantitative comparison among the four storm datasets. Each pre-storm bathymetry, hourly wave data, and water level observed at microtidal, wave-dominant, and straight beaches in East Korea (Maengbang beach) were used for the model setup. The analysis was conducted based on the Brier Skill Score (BSS) [26], and the likelihood of BSS [6] was calculated using the observed and modeled bed-level changes.

The remainder of this paper is organized as follows. The study area and multiple storm datasets are described in Section 2. The methodology used for the numerical setup, model calibration, and detailed analysis is provided in Section 3. Section 4 comprehensively describes the results based on a quantitative comparison. Section 5 presents a discussion and conclusion of the study.

2. Field Data

2.1. Study Area

Field observations and numerical simulations were conducted at Maengbang Beach (37.40° N, 129.21° E), located between the Osip River (to the northwest) and the Maeub River (to the southeast) on the east coast of Korea. This area predominantly consists of crescentic bars, although the beach state [27] changes mainly under intense storm waves of long durations (Figure 1). The study site is a straight and open coastline facing northeast (NE; approximately 41.6°). The length of the sandy beach is approximately 4.5 km, and the beach width is 50 m on average, but the difference between the minimum and maximum beach widths is approximately 100 m depending on the development location of the crescentic bars; therefore, it has a large fluctuation range at each point. The average slope of the upper shoreface (between -10 m depth and 0 m contours) was 0.025 (gentle), while the beach face slope was 0.15 (steep). The median grain size in this area is seaward fining from about 0.65 mm (near mean sea level, MSL) to 0.25 mm (nearshore), resulting in approximately 0.4 mm on average. This beach is microtidal (mean high water level (MHHWL) ~ 33.8 cm) and wave-dominant where wave incidence normal to the coastline (NE direction) prevails [28]. However, easterly and northerly waves also significantly affect the development of wave-induced currents, sediment transport, and the location of crescentic sandbars.



Figure 1. (a) Maengbang beach with crescentic bars; and (b) longshore uniform bar due to a series of storms (image acquired from Google Earth). The area within the red rectangle denotes the location where analysis of bathymetric data and numerical results is performed.

2.2. Storm Events

The study area is intermittently subjected to storm events driven by extratropical low-pressure and typhoon [25,29]. The features of these two factors (e.g., the intensity and path of typhoons and the distribution of atmospheric pressure causing strong winds) affect the characteristics of individual storms, such as wave height, period, direction, duration, and storm surge, resulting in different impacts on the beach/dune system [21,22] and multiple sandbar systems [12,30]. Storm clusters, a series of storms with close intervals between storms, can also occur owing to extreme atmospheric phenomena, leading to similar or more severe erosion in comparison to a single storm event with higher wave energy (longer return period) [21,22,30]. Additionally, the sequence of each storm within consecutive storms could lead to different responses to beach/dune erosion, whereas the

initial storm might have a significant impact on the response of the beach/dune system to subsequent storms [31].

As defined in [22], this study uses a threshold wave height ($H_{s, threshold}$) of 2.5 m to define an individual storm at Maengbang Beach and a time interval of 12 h between storms (IN) as a threshold to differentiate each storm. However, a storm over $H_{s, threshold}$ that lasts longer than 6 h is considered an individual storm. It should be noted that if a storm event with a water level (tide + storm surge) that exceeds MHHWL (0.34 m), and the storm duration is less than 6 h, it is also considered a storm condition because the storm impact can also be aggravated by storm surges. The recovery period was set as one month, the same period as in [22], in light of the analysis of periodic bathymetry surveys conducted over four years at this site. Therefore, storm events with a $12\text{ h} < \text{IN} < \text{recovery period}$ belong to clustered storms. With the above definition of a single storm and storm cluster, we use the storm power index (see [22] for more details) S_{pi} as a function of discretized storm duration (ΔD) and wave height (ΔH_i), to quantify the strength of a storm event:

$$S_{pi} = \sum_{i=1}^m (\Delta D \times \Delta H_i^2). \tag{1}$$

The wave data observed at an acoustic wave and current profiler (AWAC at W1 in Figure 1) at a water depth of 30 m from March 2017 to September 2020 produced four storm datasets (S1, S2, C1, and C2), including the significant wave height H_s , peak wave period T_p , and peak wave direction D_p (clockwise from true north). Figure 2 shows the time series of wave height (solid blue line) and wave direction (green circle) collected before and after the storm bathymetry for each storm condition. The period that satisfies the aforementioned storm definitions indicates an individual storm condition (gray bar), classifying two single storm events (S1 and S2) and two clustered storm events (C1 and C2).

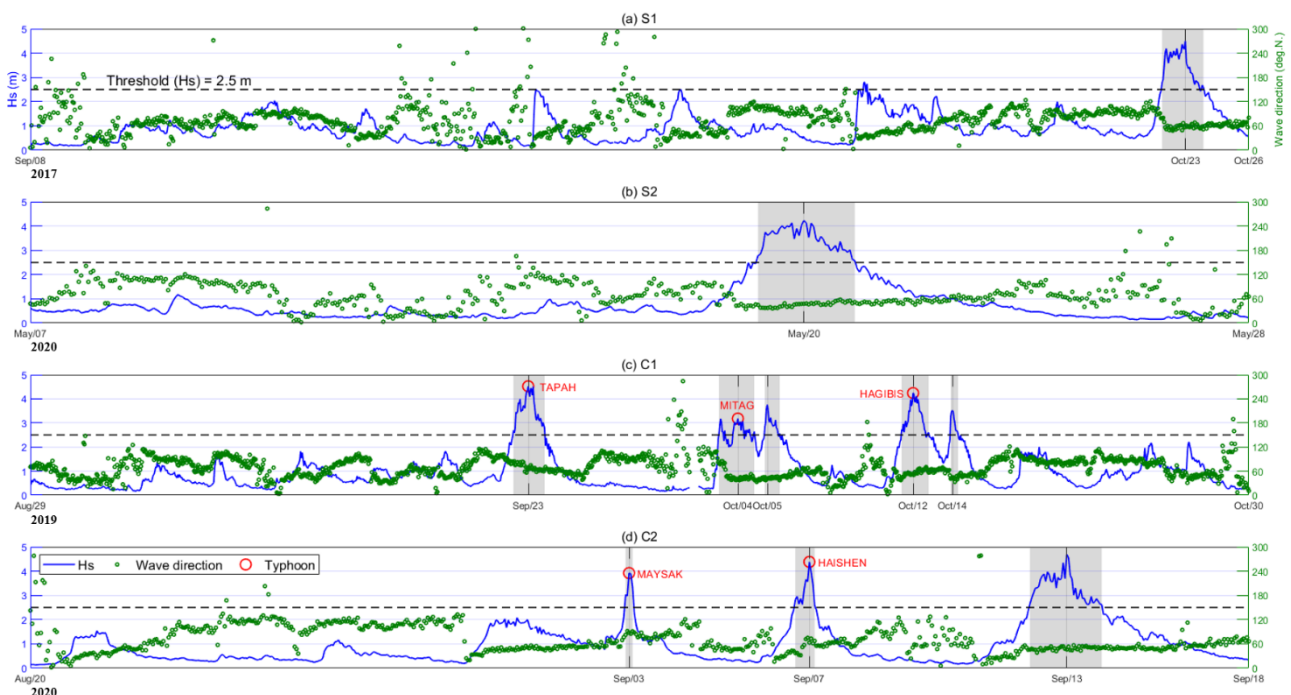


Figure 2. Time series of significant wave height (solid blue line) and wave direction (green circle) collected between pre- and post-storm bathymetry for each storm condition (S1 (a); S2 (b); C1 (c); and C2 (d)). The red circles indicate when typhoons affect the study area (Maengbang beach).

Bathymetric surveys were conducted before and after each storm event using RTK-GNSS (GX1230 and Viva GS16, Leica) for topography (MSL to MSL(+) 6 m) and high-precision GNSS and echo sounder (AquaRuler 200S, MIDAS) for nearshore and foreshore bathymetry (MSL (–) 25 m to MSL). Long-term topography and bathymetry surveys are ongoing as part of the fundamental data provision for coastal erosion control and countermeasures. Bathymetric data available for storm events showed that the depth of closure (DoC) in this study was MSL(–) 10 m because even when five consecutive storms impacted the study area (C1) with the largest storm power of $508 \text{ m}^2\text{h}$, no morphological changes occurred at the water depth. This study collected bathymetric datasets and interpolated them into the numerical grid (see Section 3.1 for further details on the grid). The analysis was performed in the central part of this study area (within the red rectangle in Figure 1a), ranging approximately 1500 m in the alongshore direction to focus on relatively natural sandy beach by neglecting other impacts that stem from engineering structures (construction started in 2020 on the northwest side of Maengbang beach) and the sand inflow by the Maeub River (Figure 1).

Figure 3 shows the subaerial volume changes according to the cumulative storm power (dark triangles) for each event (S1 to C2). The subaerial beach in this study extends between MSL to fixed boundaries (i.e., coastal road). The measured values are separately plotted as the average erosion subaerial volume changes ($\overline{\Delta V}$, light green triangles in Figure 3) and outside of two standard deviations ($\overline{\Delta V}_{2\sigma}$, green bars in Figure 3) to differentiate the average and extreme impacts of volume changes on storm events. The subaerial volume change was calculated by subtracting the post-storm profile volume from the pre-storm profile volume. For calculating average erosion subaerial volume change, this study used 62 (S1), 72 (S2), 60 (C1), and 83 (S2) erosive profiles out of 121 profile data. Although the storm powers of individual storms consisting of storm clusters are similar or smaller than those of single storms (Table 1), $\overline{\Delta V}_{2\sigma}$ (dramatic erosion volume change) tends to increase with cumulative storm power. However, $\overline{\Delta V}$ (average erosion volume change) exhibits no significant differences with varying cumulative storm power ($12.8\sim 17.1 \text{ m}^3/\text{m}$) compared to $\overline{\Delta V}_{2\sigma}$ ($30.4\sim 48.2 \text{ m}^3/\text{m}$). These differences stem from the equilibrium profile response [32–34], indicating that beach responses can differ according to precedent morphology (e.g., beach width). Figure 4 shows the volume changes after storm events depending on the beach width observed in the pre-bathymetry survey, illustrating that the initial wide (narrow) beach width is likely to be more eroded (accreted). The present study area generally follows the equilibrium concept, and accretions were observed regardless of the storm power of each event when deviations of beach width were less than -10 m . In addition, Figure 5 indicates that the shoreline changes in response to each storm condition also tend to be correlated with the location of the nearshore crescentic sandbars. The mean bathymetry (Figure 5a) calculated from the collected bathymetric data indicates the predominance of crescentic sandbars, as shown in Figure 1a, but the bar locations continuously changed with time in response to storm events. For instance, the crests of the sand bar located around MSL(–) 2 to 4 m (blue asterisks in Figure 5d) moved to MSL(–) 4 m (red asterisks in Figure 5d) after C1, turning the initial crescentic sandbar into a longshore uniform sandbar. Consequently, compound processes by the equilibrium concept and crescentic sandbars affect the beach response at this study site, but consecutive storm events mainly impact extreme erosion. In the following section, we present further details on the classified storm events and bathymetric surveys available for these events, which are summarized in Table 1.

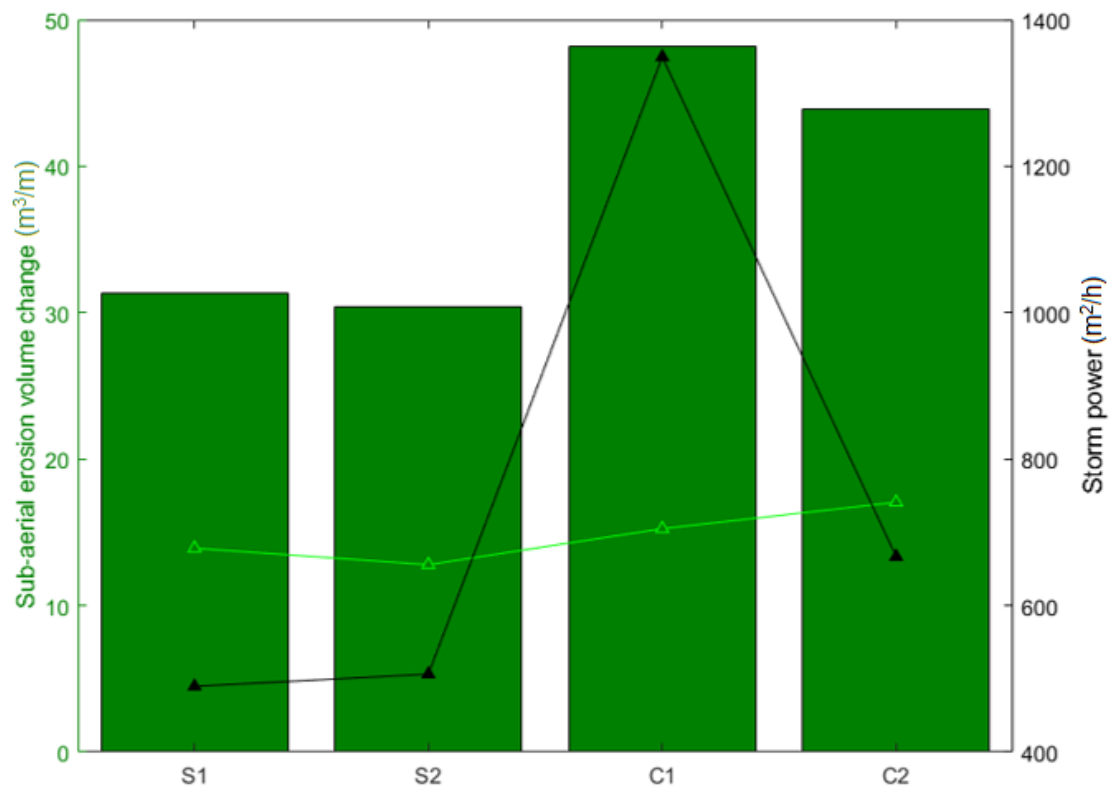


Figure 3. Average subaerial volume changes according to cumulative storm powers (dark triangles). The light green triangles and green bars indicate the average subaerial erosion volume change and that outside of the two standard deviations, respectively.

Table 1. Summary of the classified storm events (S1 to C2) and bathymetric surveys available for these events.

Storm Event	Time Interval between Bathymetric Survey (Days)	Pre-Storm Survey (Days before Initial Storm Starts)	Post-Storm Survey (Days after Final Storm Ends)	Number of Storms	Each Storm Duration (Hours)	Each Storm Power (m²h)	Cumulative Storm Power m²h	Characteristics at Each Storm Peak Hs			
								H _s (m)	T _p (s)	D _p (deg. N)	Water Level (m)
S1	2017-09-08~10/26 (48)	44.6	1.8	1	38	490	490	4.5	10.2	57.1	−0.25
S2	2020-05-07~05/28 (21)	11.7	6.8	1	59	506	506	4.2	11.5	47.6	0.19
C1	2019-08-29~10/30 (62)	24.6	14.8	5	39	508	1350	4.5	10.9	69.1	−0.03
					27	218		3.2	10.1	40.5	0.34
					18	167		3.8	10.7	42.1	0.17
					32	363		4.2	10.5	53.4	−0.12
C2	2020-08-20~09/18 (29)	14.2	3.5	3	5	60	667	3.9	9.3	87.8	0.83
					12	129		4.4	10.4	63.0	0.39
					42	478		4.7	11.4	46.2	0.06

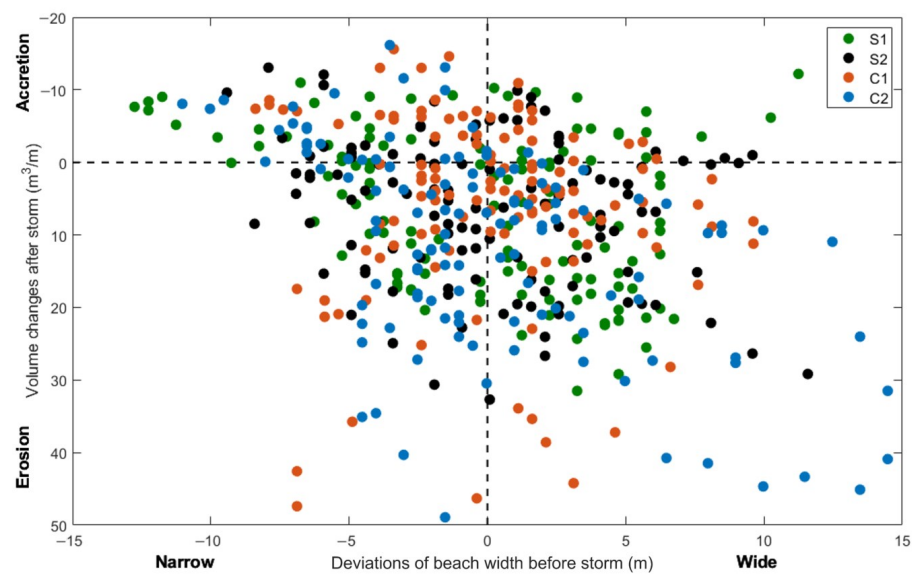


Figure 4. Subaerial volume changes according to beach width observed at the pre-bathymetry survey at each storm condition (S1 to C2).

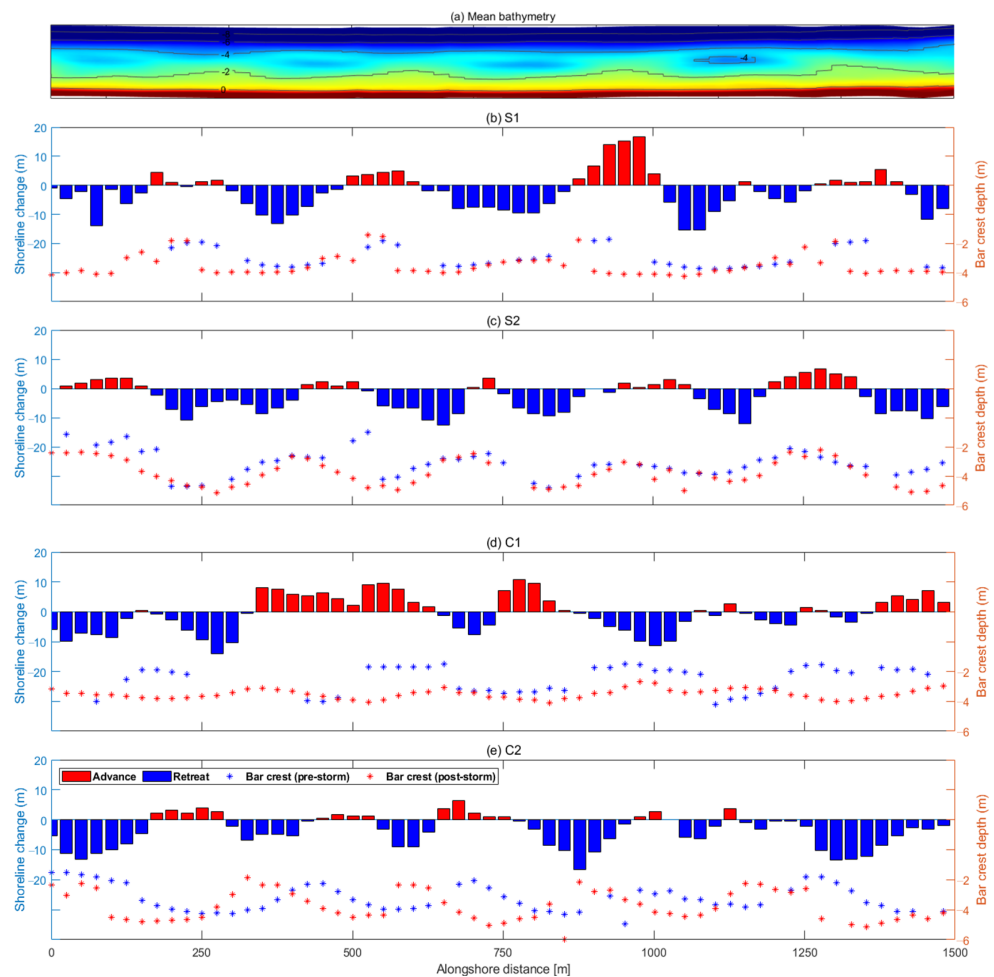


Figure 5. Compared to the mean bathymetry (a), migration of nearshore crescentic sandbars and shoreline change in response to each storm event (b–e). Blue and red bars (asterisks) denote the shoreline retreat (depth of bar crests pre-storm) and advance (depth of bar crests post-storm), respectively.

2.2.1. S1

On 10 October 2017, H_s exceeded $H_{s, threshold}$ (2.5 m), but this event was neglected for a storm condition because it lasted only 3 h ($D < 6$ h). In addition, the first three storms with more than 2 m wave height would have affected final profile changes. However, field observation right after the three events was not conducted since repeated bathymetric surveys with short-term intervals are impractical at most sites. Therefore, it is impossible to investigate the effect of those events on profile change. We considered that those effects do not have significant impacts on overall profile changes compared to the last intensive event because of the short duration. There were also a few weeks for the beach to recover even if it affected the changes. Consequently, we assumed that those first three events are not remarkable on profile changes compared to the much higher wave energy with a long duration and considered S1 as a single event.

The first single storm event (S1) recorded a storm power of $490 m^2h$ with an incident wave of 57.1° at the peak storm wave height, and it lasted for 38 h from 22 to 24 October 2017. Average subaerial erosion volume change outside of the two standard deviations ($\overline{\Delta V_{2\sigma}}$) was $31.3 m^3/m$, while average subaerial erosion volume change ($\overline{\Delta V}$) was $13.9 m^3/m$ in response to this single storm (Figure 3). Figure 5 shows that the length and amplitude of the crescentic sandbars increased after the storm event, along with the tendency of out-of-phase coupling with the shoreline (erosive megacusps facing the lee side of the sandbar embayment), which has been found in many sandy beaches with crescentic bars [11,12,30,35].

2.2.2. S2

The second single storm event (S2) spanned 59 h, recording the most prolonged storm duration among the individual storms in the collected storm datasets; therefore, it had similar storm power of $506 m^2h$ to that of S1, despite the slightly lower peak storm wave height (4.2 m). The incident wave was predominantly normal to the shoreline (47.6°) at storm peak H_s . The average $\overline{\Delta V_{2\sigma}}$ and $\overline{\Delta V}$ were 30.4 and $12.8 m^3/m$, comparable with those of S1 (Figure 3). The locations of crescentic bars showed no significant change, while cross-shore migrations of the sandbars were observed, deepening the depth of the bar crests (Figure 5c). Interestingly, a similar out-of-phase relationship between the shoreline and crescentic bars was discovered for S1, although both S1 and S2 had different hydrodynamics and precedent morphologies during the storm events.

2.2.3. C1

The seven typhoons in 2019 directly and indirectly affected the country. Among them, three typhoons that mainly affected the study area in September and October 2019 were of two types in terms of wave direction [25] (ENE and NE waves (Table 1)), leading to five storm events in a storm cluster (C1). A series of storms started with the largest storm power ($508 m^2h$) lasting 39 h with a peak storm wave height (4.5 m) comparable to the S1 event. The first event in C1 was dominantly ENE wave groups under the effect of Typhoon Tapah, which induced longshore sediment transport toward the northwest of the area [25]. The second and third storm events in C1 induced by Typhoon Mitag recorded storm powers of 218 and $167 m^2h$ due to relatively low wave height (≤ 3.8 m) and short duration (≤ 27 h) compared to the S1 and S2 events. However, Typhoon Mitag passed directly through the study site, reaching the MHHWL (0.34 m) owing to the storm surge. The next two storms, with storm powers of 363 and $94 m^2h$ occurred under the influence of Typhoon Hagibis. The typhoon passed through the east coast of Japan, but it was classified as a super typhoon (Korea Meteorological Administration, KMA) with a diameter of approximately 1400 km and a Category 5 on the Saffir-Simpson Hurricane Scale (SSHs). After the C1 event, dramatic erosion profiles were observed with the averaged $\overline{\Delta V_{2\sigma}}$ of $48.2 m^3/m$, while $\overline{\Delta V}$ was $15.3 m^3/m$, which is slightly larger than single storm conditions (S1 and S2). This result shows that the equilibrium profile response reduced the gap between the averaged subaerial erosion volume ($\overline{\Delta V}$) and that of S1 and S2. In addition, the cumulative impacts of five consecutive storms (cumulative storm power of $1350 m^2h$) caused extreme erosion, but

the amount of erosion was not proportional to the storm power owing to the equilibrium beach response. Previous numerical results [25] showed that the first largest storm in C1 eroded this study area for the most part, and subsequent storm events had relatively small impacts compared to the first one in terms of subaerial erosion, as reported by [22]. As a result of a cluster of storms, the rhythmic beach bar transformed into a longshore bar, although the state had a repeated pattern of erosive and accretive profiles near the MSL (Figures 1b and 5d).

2.2.4. C2

Two typhoons, Maysak and Haishen, made landfall on the east coast of Korea and led to three storm events in a storm cluster (C2), causing considerable loss of sediment despite the short storm duration (5 and 12 h, respectively) during the first two storms. However, wave heights during the storms were sufficiently high to cause coastal erosion, and the water level (0.83 and 0.39 m) exceeded MHHWL (0.34 m) as a result of the storm surge. Although the storm duration of the first storm in C1 was less than 6 h, it was regarded as a storm because the water level (0.83 m) outweighed the MHHWL. The third storm in C1 with a storm power of $478 \text{ m}^2\text{h}$ recorded the highest peak storm wave height (4.7 m) with mainly a NE wave direction for a period of 42 h, which was relatively long compared to the previous two storms. Consequently, severe erosion profiles were discovered with the averaged $\overline{\Delta V_{2\sigma}}$ of $43.9 \text{ m}^3/\text{m}$, while $\overline{\Delta V}$ was $17.1 \text{ m}^3/\text{m}$, similar to the C1 event. Extreme erosion was observed only when deviations of beach width before C1 were wider than -5 m . Although the individual storm powers in the cluster storm (C2) were lower than those of the single storm events (S1 and S2), $\overline{\Delta V}$ after C2 was larger than that of S1 and S2. As shown in Figures 3 and 4, a storm cluster composed of several storms with small storm powers (C2) could result in more damage (e.g., coastal erosion) than that from a single storm with a larger storm power (S1 and S2) [21,22]. Crescentic sandbars migrated in the longshore direction mainly due to the ENE and E storm waves of the first two storms in C2, and the relationship between the shoreline and sandbars was mixed with out-of-phase and in-phase couplings (accretive megacusps facing the lee side of the sandbar embayment).

3. Methodology

3.1. Numerical Setup

The four aforementioned storm events were modeled in the study area using a two-dimensional horizontal (2DH) XBSB (version 1.23.5527, XBeachX) that can simulate the hydrodynamics and morphological changes in relatively narrow areas (e.g., beaches, dunes, and barrier islands) during storm wave events. To model these areas in the XBSB, hydrodynamics such as short wave, long wave, and roller energy with wave and water level input as boundary conditions were calculated first. Subsequently, morphodynamics, such as sediment transport and resultant bed-level changes, were simulated. This study used the JONSWAP spectrum with parametric variables (H_s , T_p , D_p , and directional spreading) observed in AWAC (Figure 1) for the wave boundary condition. The water level time series measured from the Korea Hydrographic and Oceanographic Agency's Donghae Port Tidal Observatory (37.49° N , 129.14° E) was also applied to the model boundaries. However, the hydrodynamic conditions used were only forced at the model boundary in the case of wave heights greater than 1 m for all simulations (S1–C2). In addition, the morphological acceleration factor (*morfac*) of 10 was used. This selective condition is intended to reduce the high computational cost derived from the relatively long intervals between pre- and post-bathymetric surveys (Table 1) and to simulate the erosive processes [36,37].

Figure 6 shows a curvilinear and non-equidistant grid established for 2D modeling, extending approximately 1.2 and 5.5 km in the cross-shore and alongshore directions, respectively. The range of both directions was expected to be consistent with the offshore boundary located at AWAC (Figure 1) and to cover the shadow zone as an easterly storm wave propagated. The size of the grid cell in the cross-shore direction varied with the

area of interest as high (2–5 m) and coarse (10 m) resolutions at beach/nearshore and in the vicinity of the offshore boundary, respectively. The grid size in the alongshore direction was nearly regular at a resolution of 12 m. The initial bottom boundary condition was set up with pre-storm bathymetric data, and grid cells that correspond with the locations of hard structures (i.e., rocks, coastal roads, and breakwaters) were considered as non-erodible layers.

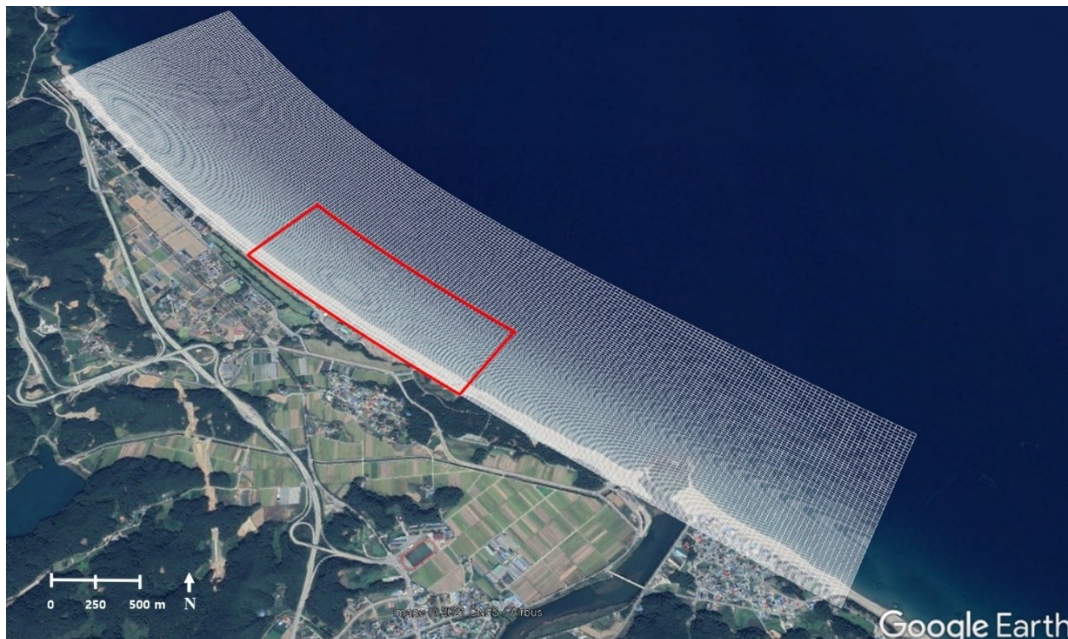


Figure 6. Curvilinear and non-equidistant grid for XBeach modeling (image obtained from Google Earth). The area within the red line, ranging from the landward tip (MSL(+) 6 m) to depth of closure (MSL(-) 10 m) in the cross-shore direction, denotes the location where analysis of bathymetric data and numerical results was performed.

3.2. Model Calibration

The XBeach model has a few empirical equations with numerous parameters that can be calibrated because of the lack of understanding of hydromorphodynamics (e.g., grain stabilization, wave breaking, and swash zone processes) and model simplification (e.g., uniform sand assumption, phase-averaged mode, and depth-averaged model). To improve the model performance under these limitations, physically based calibrations [8,19,38] and a heuristic equation [39] to complement the missing physics have been applied to the modeling of morphological changes caused by storm events in many studies. Moreover, the model has been supplemented by additional physics [20,40–42] to overcome the poor prediction skill derived from intrinsic limitations in XBSB. However, despite considerable efforts, the adjustment of free parameters suitable to the specific sites and events in modeling using the manual ‘trial-and-error’ method or the GLUE process [6,7] is unavoidable.

Simmons et al. (2017) [6] conducted a GLUE test at collision and overwash profiles in Lido Di Classe, Italy, using adjustable parameters frequently reported in the literature to find key sensitive parameters. Simmons et al., 2019 [7] used three key parameters (*facua*, *gamma*, and *bedfriccoef*) to identify the influence on calibration datasets in modeling subaerial beach storm erosion on three embayed beaches in Australia. Similarly, other studies [2,43] have predicted subaerial beach erosion by storm events using these three parameters. However, this study excluded *bedfriccoef* for model calibration as it is proved to be relatively insensitive compared to the other two parameters (*facua* and *gamma*) in the collision regime [2,43–45], which is consistent with the present study area.

XBSB provides two formulations (Roelvink, 1993 [46] and Daly et al., 2012 [42], hereafter called ‘Rv93’ and ‘RvDaly’, respectively) for the dissipation due to short wave breaking that is important for the prediction of wave transformation and run-up in the surf and swash zone. Briefly, the Rv93 formulation adopts a probabilistic approach depending on local waves and depths with two sensitive parameters (*gamma* and *alpha*). In contrast, the RvDaly formulation uses a deterministic approach, in which the occurrence of wave- and depth-induced breaking is determined as the breaking and reformation criteria (*gamma* and *gamma2*). Daly et al. (2012) [42] showed that wave dissipation simulated by the probabilistic function is underestimated in areas where the water depth rapidly varies (i.e., bar-trough system), while the discrepancy in hydrodynamics simulated by both formulations is negligible in areas with a plane slope [47]. Several studies have shown that the model performance of the RvDaly formulation is better than that of Rv93 in predicting hydrodynamics on a barred beach [48] and near a hard structure [49]. In addition, a previous study [25,50] showed better results with RvDaly formulation in simulating bed level changes triggered by the C1 event at this study site based on BSS estimation. Therefore, this study adopted four key parameters (*facua*, *alpha*, *gamma*, and *gamma2*) with the RvDaly formulation and combined each parameter to produce 96 parameter sets (Table 2). It should be noted that the default values of free parameters are used except for the parameters listed in Table 2. Consequently, this study simulated a total of 384 cases (96 parameter sets with four storm events) to identify the effect of event-specific calibration data in spatiotemporally variable bathymetry.

Table 2. Parameter descriptions and values used for calibration processes.

Parameter	Description	Values
<i>facua</i> *	Adjustable parameters for parameterizing both wave skewness (<i>facSk</i>) and asymmetry (<i>facAs</i>)	0.10, 0.15, 0.20, 0.25
<i>alpha</i> *	Wave dissipation coefficient for short wave breaking Breaker parameter in RvDaly formulation, with larger values of <i>gamma</i> encouraging less wave dissipation (See [44] for details)	1, 2
<i>gamma</i> *	Reformation parameter in RvDaly formulation, with larger values of <i>gamma2</i> encouraging less wave dissipation (See [44] for details)	0.42, 0.52, 0.62
<i>gamma2</i> *		0.25, 0.30, 0.35, 0.40
<i>D50</i>	D50 sediment diameter applied to the model domain	0.4 mm
<i>D90</i>	D90 sediment diameter applied to the model domain	0.7 mm
<i>bedfriccoef</i>	Bed friction coefficient defined as Chezy value, influencing mean flows and long waves	40 m ^{1/2} /s
<i>break</i>	Type of breaker formulation	roelvink_daly [42]
<i>form</i>	Type of sediment transport formulation	soulsby_vanrijn [51]

* Only these four parameters were combined to produce 96 parameter sets for storm events (S1–C2).

3.3. Assessment of Event-Specific Calibration Data

A quantitative comparison of the simulated and observed bed level changes for 384 cases (96 (parameter combinations) × 4 (storm conditions)) was conducted based on the BSS [26]:

$$BSS = 1 - \left[\frac{(|z_c - z_m|)^2}{(z_i - z_m)^2} \right], \tag{2}$$

where z_c , z_m , and z_i denote the computed, measured, and initial bed level, respectively. This metric can be classified as follows: 0.8 ~ 1.0 (excellent), 0.6 ~ 0.8 (good), 0.3 ~ 0.6 (reasonable), 0 ~ 0.3 (poor), and < 0 (bad). The likelihood of a BSS [6] is defined as

$$L_{BSS} = BSS_i / \sum_{i=1}^n BSS_i, \tag{3}$$

where n is the total number of calibration sets for each storm case ($n = 96$), and BSS_i is a BSS of an individual model run. This study calculates the BSS with bed elevation data

above the MSL because evaluating morphological changes in the subaerial beach is more useful for practical and protective purposes in coastal engineering projects than those in the offshore region. Therefore, many studies have focused on the measured data above the MSL in calibrating and validating the XBeach model [6,7,18,19]. The area for BSS evaluation contains 121 profile data, which span approximately 1.5 km and above MSL in the alongshore and cross-shore direction, respectively. BSS is a direct proxy for quantifying the model performance at a given reference prediction (i.e., observed bed level changes), with higher values indicating more accurate prediction (maximum BSS = 1). Although BSS represents the objective model performance with a numerical value for a parameter combination, L_{bss} quantitatively explains the weight of individual skills in the whole model skill distribution by rescaling the sum of the likelihood to one (higher values indicate higher skill than others). It should be noted that L_{bss} is set to 0 when the BSS of a model run is less than 0, as in [6]. This study uses both metrics to quantitatively analyze the general model performance, sensitivity of each parameter set, and reliable parameter ranges for varying storm events.

4. Results

4.1. Influence of Event-Specific Datasets on Model Calibration

Figure 7 shows the ratio of the erosion/accretion profile and model skills under all storm conditions to investigate XBSB's limitation to simulate the accretion process within given parameter combinations ($N_s = 96$). Figure 7a indicates that the erosion profiles were relatively dominant after S2 and C2 (59.5% and 68.6%, respectively), whereas the erosion and accretion profile ratios after S1 and C1 were nearly half. Although the cumulative storm powers of C1 and S1 were the largest and smallest, respectively, the number of erosion profiles was disproportional to the cumulative storm power. Figure 7b and c show the ratio of model skill corresponding to $BSS \geq 0.3$ (reasonable) out of 96 simulations for each storm event. We considered erosion, accretion, and all profiles ($N_p = 121$, both erosion and accretion profiles) for calculating each ratio under the given parameter combinations. The ratios of model skill ($BSS \geq 0.3$) in the erosion profile were 87.5% (S1) and 63.5% (S2), showing good performance in varying parameter sets. However, the ratios of parameter combinations with a BSS higher than 0.3 were reduced to 44.8% (C2) and 13.5% (C1). This indicates that 84 parameter sets showed good model results in S1, whereas only 13 parameter sets presented reliable results in C1. These results imply that relatively low ratios in clustered storm events signify poor overall model performance or limited applicability to specific parameter sets within a given parameter range. Additionally, many parameter sets show consistency with erosion profiles, but the reasonable model skill is less than 5% in all profiles because none of the parameter combinations exceeded the BSS of 0.3 in accretion profiles. Consequently, this study focused on erosive areas for further analysis because XBSB calibrated from either erosive or accretive events has limitations in simultaneously predicting erosion and accretion cases.

Figure 8 shows a comparison of the BSS calculated for each storm event, and the corresponding points on both axes are plotted when different storm conditions with the same parameter set are used. When calibrated by single storm events (S1 and S2), many given parameter sets showed better model performance (Figure 8a) than those with calibration by cluster storm events (C1 and C2 in Figure 8b). In other words, the dependable model performance under cluster storm conditions was found to be more limited than that under single storm conditions. Each point also indicates the applicability of a parameter set calibrated for one storm event to a different storm event. When the calibrated set with BSS above 0.3 in C1 or C2 is applied to S1 or S2, most parameter sets lead to reasonable model predictions with BSS above 0.3 (Figure 8c–f). However, a BSS below 0.3 can be found in C1 or C2, although the calibrated set by S1 or S2 shows a BSS above 0.3 (Figure 8c–f). Reliable model skills in any storm event tend to be produced as BSS is higher than 0.3 in clustered storm events (i.e., BSSs above 0.3 plotted on both axes are mainly observed if BSSs calculated in C1 or C2 are higher than 0.3). In contrast, a random parameter set calibrated

by a single storm condition has a relatively low probability of exhibiting high model performance under any condition. This finding suggests that the XBeach area model in XBSB is event-specific in terms of calibration data, and the optimum parameter set calibrated by relatively lower cumulative storm power (e.g., S1 and S2 in the present study) could not be applied to the modeling of different storm events, even at the same site. One can expect that severe wave conditions would have small variability in selecting the optimum parameter values, resulting in acceptable model performance. Therefore, the modeler can have different levels of certainty to determine an optimum parameter set, depending on the cumulative storm power. This is important because a random parameter combination that does not represent real physical processes can generate good model performance, which leads to incorrect decision making in the calibration process.

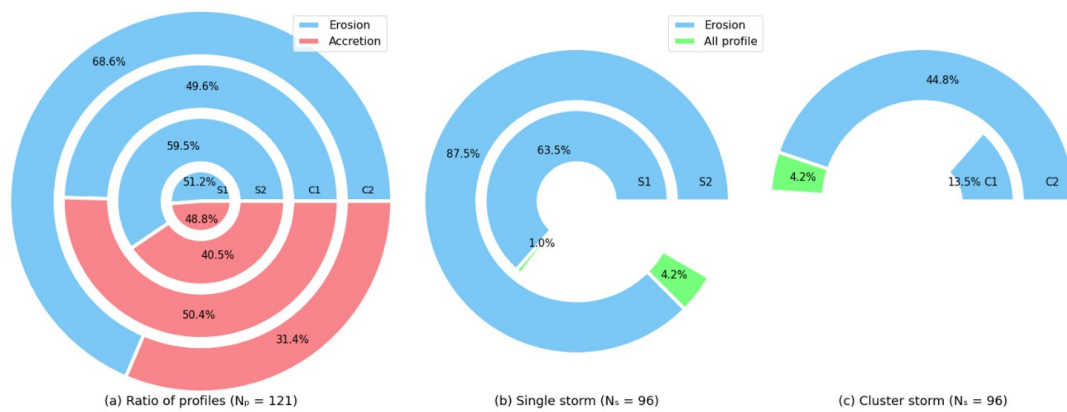


Figure 7. Ratio of erosion (blue) and accretion (red) profiles out of the total number of profiles ($N_p = 121$) (a) and the ratio of model skill, corresponding to $BSS \geq 0.3$ out of 96 simulations ($N_s = 96$) for single storm (b) and cluster storm (c) events. These ratios are calculated in erosion (blue), accretion (red), and all 121 profiles (green), respectively. It should be noted that none of the BSS calculated in accretion profiles exceeds the threshold value (0.3).

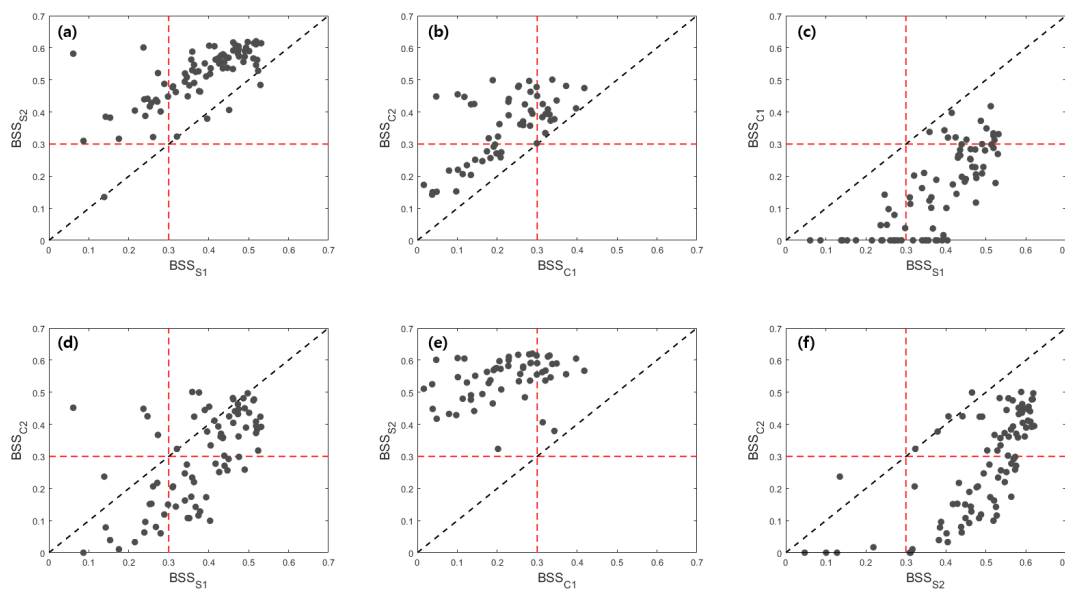


Figure 8. Comparison of BSS calculated in each storm condition (S1 and S2 (a), C1 and C2 (b), S1 and C1 (c), S1 and C2 (d), C1 and S2 (e) and S2 and C2 (f) when the BSS on the x -axis is higher than 0. It should be noted that BSS is plotted as 0 if BSS on the y -axis is 0 or lower for clarity. The red dashed line indicates the threshold value of reasonable model performance [26] ($BSS = 0.3$).

Figure 9a shows the likelihood distributions of each storm event cumulated in descending order (i.e., higher likelihood is first cumulated). The Kolmogorov–Smirnov (K-S) D statistic [6,52] was used to analyze quantitative model sensitivity to parameter combinations depending on storm conditions. The K–S D statistic is calculated by the maximum distance between the cumulative likelihood curve condition and the uniform likelihood distribution and ranges from 0 to 1 with the higher value indicating more sensitive model results within the same parameter space under respective storm conditions. It should be noted that the uniform likelihood distribution (dashed line in Figure 9a) denotes the same BSS value in all 96 parameter sets (i.e., no variation of BSS depending on random parameter combinations).

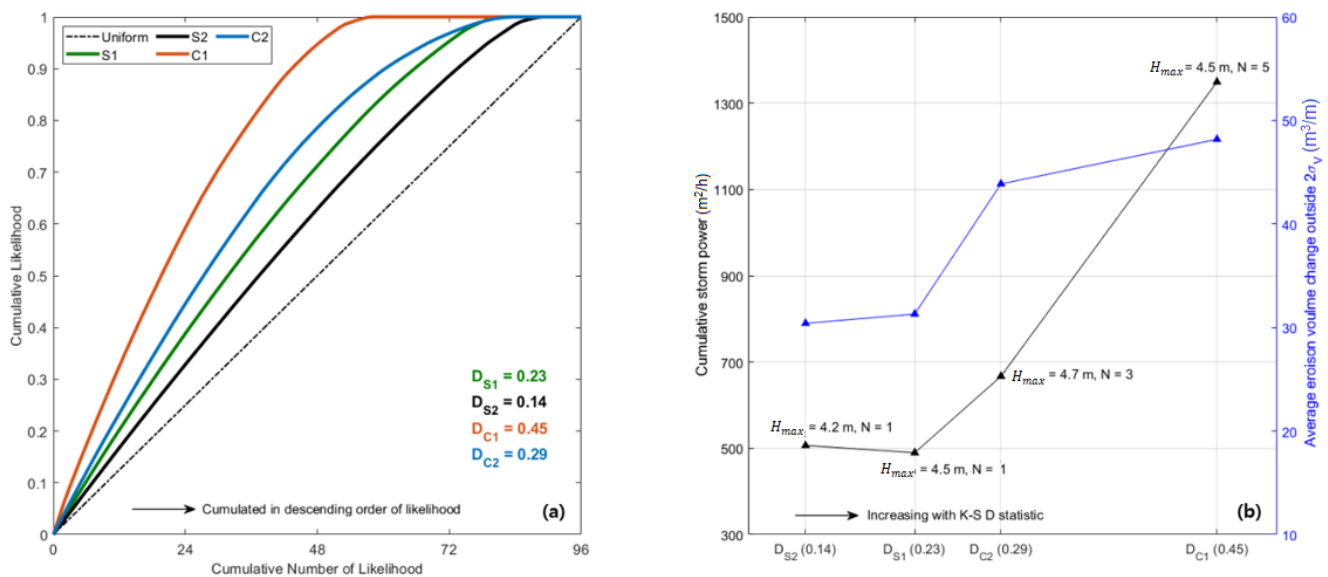


Figure 9. (a) Cumulative likelihood distributions in each storm condition with the K–S D statistic; and (b) model sensitivity based on K–S D to the cumulative storm power and the average erosion volume change outside the two standard deviations ($\overline{\Delta V_{2\sigma}}$); H_{max} and N indicate the maximum storm wave height during each storm event and number of storms in a cluster, respectively; higher K–S D indicates a higher model sensitivity to parameter sets.

A relatively small number of parameter sets in clustered storm events tended to occupy a higher BSS among the total BSS distribution (Figure 8), which means that with fewer parameter combinations, the cumulative distribution in those events was higher than that in single storm events (Figure 9a). Under the complex bathymetry in the present study, C1 was ranked as the most sensitive condition for model performance at a given parameter range based on the K–S D statistic, while C2, S1, and S2 were ranked in subsequent order. Figure 9b compares the quantitative measures of the model sensitivity with each cumulative storm power and the observed $\overline{\Delta V_{2\sigma}}$. As shown in Table 1 and Figure 3, the cumulative storm powers and $\overline{\Delta V_{2\sigma}}$ values proportionally increase with the number of storms in each event. Similarly, the model sensitivity to parameter sets positively correlates with the cumulative storm power and $\overline{\Delta V_{2\sigma}}$, although the maximum storm wave heights during all storm conditions are comparable (Table 3). In particular, reliable model results tend to be limited to a small number of parameter sets as the observed $\overline{\Delta V_{2\sigma}}$ increases. In the selection of an event-specific dataset for calibration, the modeler has certain ambiguity regarding which storm event to select when individual storm powers of a cluster storm are less than or similar to a single storm power, as applicable to the present study. Consequently, if one event-specific dataset contains extreme erosion volume changes due to cumulative storm power compared to a single storm event, a clustered storm event is required to obtain reliable model results in that study area. Interestingly, the wave direction and pre-storm beach state were all different depending on the storm conditions (Table 1 and Figure 5). In

addition, S1 and C1 had relatively longer time intervals between the bathymetric surveys than S2 and C2. Incident wave directions and survey intervals considerably impact the calibration parameters because they are closely related to hydro-morphodynamics during the XBeach simulation. However, these factors at the study site were not correlated with model sensitivity to parameter combinations (i.e., the K-S D value in Figure 9), as shown in Table 3. Hence, the cumulative storm power or resultant severe beach erosion may be a prior consideration in the area model of XBSB in selecting the calibration data compared to other factors because of its relatively low sensitivity.

Table 3. Comparison between model sensitivity based on K-S D and other factors based on observations.

Storm Events	S2	S1	C2	C1
Number of storms	1	1	3	5
K-S D	0.14	0.23	0.29	0.45
Cumulative storm power (m^2h)	506	490	667	1350
Maximum H_s (m)	4.2	4.5	4.7	4.5
$\Delta V_{2\sigma}$ (m^3/m)	30.4	31.3	43.9	48.2
D_p (deg. N)	47.6	57.1	87.8, 63.0, 46.2	69.1, 40.5, 42.1, 53.4, 42.5
Interval between bathymetric survey (Days)	21	48	29	62

4.2. Parameter Sensitivity

To analyze the model sensitivity with key parameters, the present study investigated the likelihood values of each parameter (*facua*, *alpha*, *gamma*, and *gamma2*) that produced 96 parameter sets for each storm condition. Figure 10 shows the sum of the likelihood values for each calibration parameter. All likelihood values are summed if a value is constant regardless of the parameter values. For instance, all likelihood values corresponding to *facua* of 0.1, even with different combinations of other parameters (*alpha*, *gamma*, and *gamma2*), are summed, with large differences in the sum indicating high model sensitivity to a certain parameter.

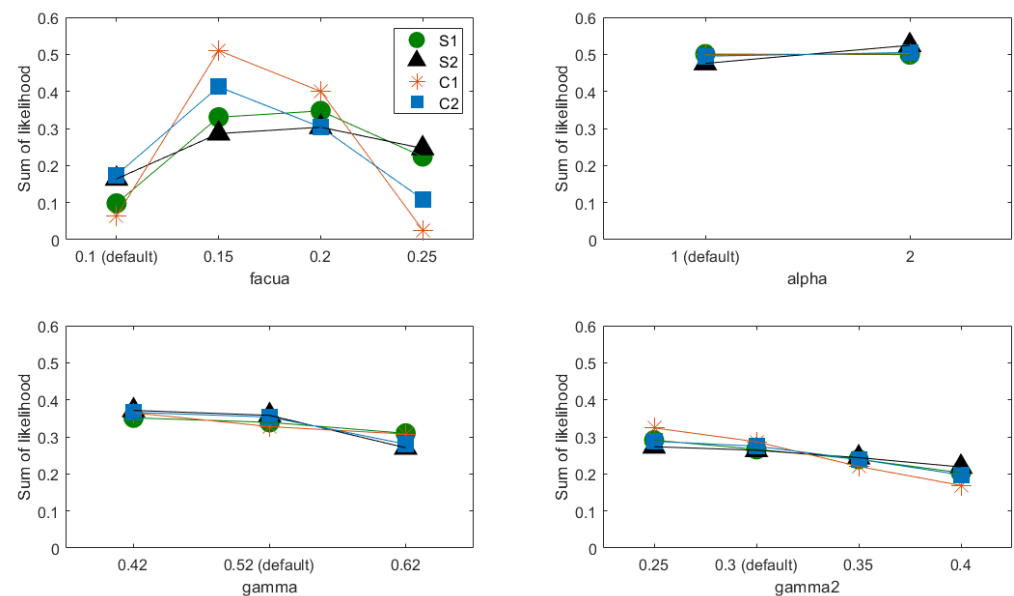


Figure 10. Sum of the likelihood at given ranges of each key parameter (*facua*, *alpha*, *gamma*, and *gamma2*). The higher sum of likelihood indicates that higher BSS values are distributed at the parameter value. In addition, a large variance of the sum of likelihood distribution indicates a high model sensitivity within given parameter combinations and incident wave conditions.

Consequently, *facua* is found to be the most sensitive parameter in modeling storm erosion, while other parameters relevant to wave dissipation have no remarkable differences in the sum of likelihood within the given parameter spaces. They are largely affected by the variation in *facua* value because of their lower sensitivity than *facua*. In other words, any value of these three parameters at a given parameter range can result in a similar model performance with different parameter combinations. Several studies [8,17,19,20] also showed a higher sensitivity of *facua* than other parameters and therefore used it differently from incident wave conditions and precedent bathymetries in the calibration process. Similarly, higher likelihood values tend to be densely distributed in *facua* of 0.15 and 0.2 in storm clusters (C1 and C2), resulting in a higher sum of the likelihood, while the model performance of the default value (*facua* = 0.1) is comparatively poor under all conditions. The distribution of the sum of likelihood flattens for single-storm conditions (S1 and S2) because likelihood values have relatively low variance throughout *facua* values. Consequently, the sensitivity of *facua* is found to be proportional to the cumulative storm power, indicating that a larger storm power may narrow down the parameter space of *facua* to produce reliable model results. The best performance (based on the highest sum of likelihood) in this study area is derived from higher values of *facua* (0.15 and 0.2 in storm cluster and single storm conditions, respectively) than its default.

Figure 11 shows the additional analysis of the other three parameters (*alpha*, *gamma*, and *gamma2*) at fixed *facua* values and indicates that the model sensitivities of each parameter vary with increasing *facua* values. These three parameters were found to be highly dependent on the changing *facua* values owing to the large influence of *facua* on sediment transport induced by incident waves. Parameter *alpha* shows a tendency to be negatively correlated with the wave shape parameter. A higher *alpha* reduces beach erosion by inducing significant wave dissipation before they reach the shoreline, compensating for the excessive erosion caused by the lower *facua*. In contrast, higher *gamma* and *gamma2* trigger beach erosion by letting waves break at shallower depths and reforming the breaking waves earlier, complementing the extensive accretion derived by higher *facua*. However, the interrelated feature between parameters weakens as excessive beach accretion occurs with the highest *facua* of 0.25, and any parameter combination results in poor model results at this point. Thus, the *facua* range for calibration processes can be readjusted to lie between 0.1 and 0.2 for other XBeach applications of erosive events at the present site. Overall, the wave shape parameter has a predominant effect on modeling subaerial storm erosion compared to the other three key parameters.

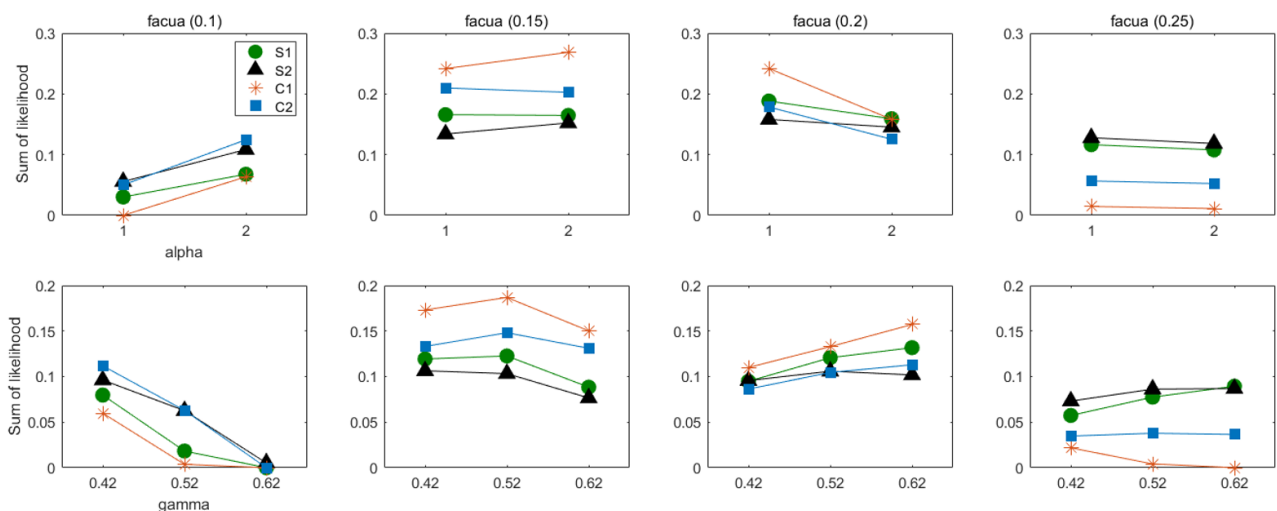


Figure 11. Cont.

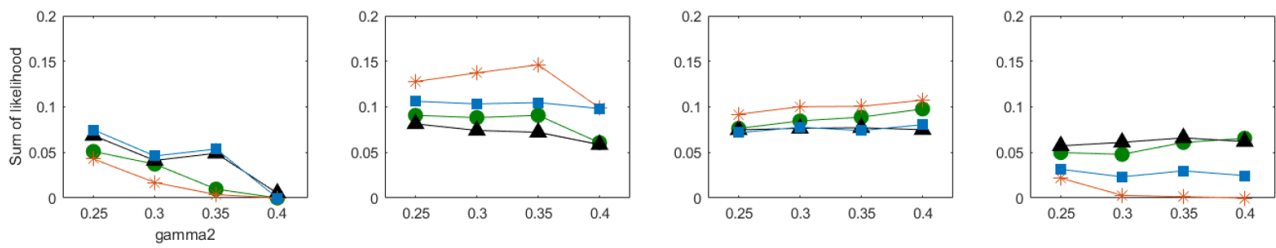


Figure 11. Sum of the likelihood of three key parameters (*alpha*, *gamma*, and *gamma2*) at each fixed *facua*. The higher sum of likelihood indicates that higher BSS values are distributed at the parameter value. In addition, large variance of the sum of likelihood distribution indicates a high model sensitivity within given parameter combinations and incident wave conditions.

4.3. Prediction of Profile Changes after Storm Events with an Optimum Parameter Set

The other three key parameters (*alpha*, *gamma*, and *gamma2*) showed a comparative insensitivity of model performance compared with *facua*, as shown in Figures 10 and 11. In all storm events, the most reliable model results are mainly found when *facua* of 0.15 is used despite equifinality (i.e., various parameter sets can reach the same desired results) induced by different parameter combinations, especially in single storm conditions in this study. If the modeler can produce reliable model performance with only one key parameter (e.g., *facua*) with the remaining parameters as default, it is a very practical way for many XBeach applications on site, regardless of any calibration dataset, also leading to a low computational cost. Figure 12 shows the simulated profile with a calibrated key parameter (*facua* of 0.15) after each storm event (S1 to C2) in comparison with the observed profile changes. As shown in Figure 3, the observed profiles show an equilibrium profile response with different volume changes according to the initial beach state. The erosion tendency in response to storm waves was reduced when the initial beach width was narrow.

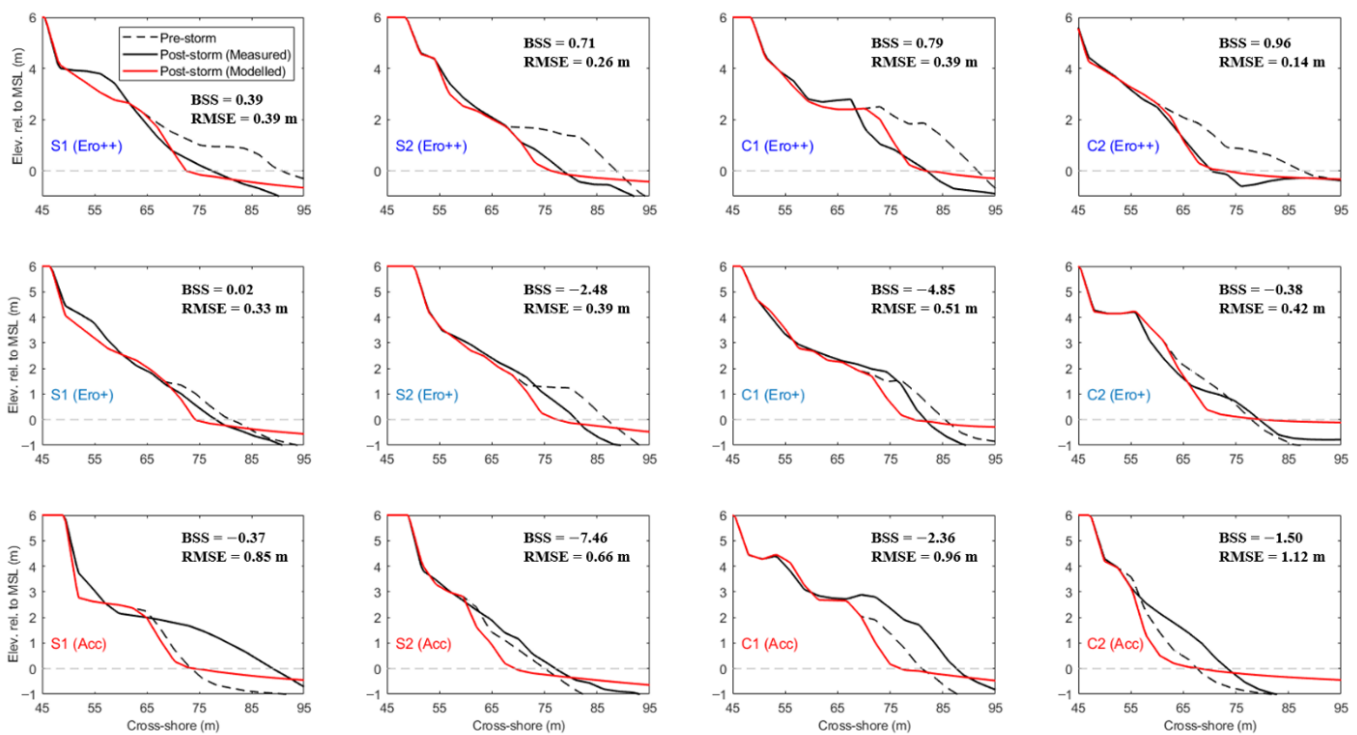


Figure 12. Model results of profile changes from the chosen parameter set (*facua* = 0.15, *alpha* = 1, *gamma* = 0.52, and *gamma2* = 0.3) under different storm conditions and initial beach widths. Ero++, Ero+, and Acc denote severe and mild erosion and accretion after storm events. BSS and RMSE are calculated by profile data above MSL.

The area model with the selected parameter set ($facua = 0.15$, $alpha = 1$, $gamma = 0.52$, and $gamma2 = 0.3$) captured the equilibrium concept well. However, the sediment transport does not move up to the subaerial region, even though the model prediction does not produce considerable change in the accretion profiles. This led to poor model performance when considering all profiles alongshore for BSS estimation, as shown in Figure 7b and c. However, the differences in the amount of erosion regarding the initial beach width are well predicted despite slight overestimation of profile changes when small erosion occurs (middle panel in Figure 12). Employing the area model instead of the profile model eliminates the uncertainties induced by profile-specific calibration in such complex bathymetry. Furthermore, choosing the least number of calibration parameters reduces the equifinality induced by various calibration combinations within event-specific calibration data.

5. Discussions and Conclusions

The present study adopted a process-based numerical model (XBeach area model) with a phase-averaged wave mode to examine the influence of event-specific calibration data on subaerial storm erosion with four adjustable parameters ($facua$, $alpha$, $gamma$, and $gamma2$). Field data and numerical simulations were conducted at Maengbang Beach, located on the east coast of Korea, where complex bathymetry and shoreline undulation are common. According to the definition of the storm power index, a function of wave height and storm duration, four storm events (two single storms and two clustered storms) impacted the study area during the field survey period, resulting in different changes in the shoreline, volume, and location of crescentic bars. Although beach erosion was observed with similar averaged subaerial volume changes after all storm events, drastic erosion volume changes were observed after storm clusters owing to accumulated storm impacts. Meanwhile, the volume changes tended to vary with the initial beach states in response to incident storm waves (i.e., a wider beach width before storm events indicates greater vulnerability to storm impacts).

The key parameters in XBeach should be adjusted to simulate appropriate hydro- and morphodynamics for a specific area of interest, leading to site- and profile-specific calibration processes. In such a complex hydro-morphodynamic environment, the area model is preferable to the profile model because it eliminates the possible uncertainty induced by profile-specific calibration. A comparison of the BSS calculated for each storm event revealed that a similar and good model performance was produced by a larger number of parameter combinations under single storms. In contrast, for clustered storm events, the limited number of calibration sets led to reliable model skill (i.e., higher model sensitivity to different parameters). Parameter sets calibrated by storm clusters have a higher probability of leading to high model skills under any storm condition. In addition, the level of model sensitivity to each storm event was positively correlated with cumulative storm power and severe erosion volume change. Reliable model results tend to be limited to a small number of parameter sets as the observed $\overline{\Delta V_{2\sigma}}$ and cumulative storm power increase. These results suggest that datasets containing drastic erosion volume changes due to cumulative storms are required for the selection of a relatively representative parameter set for the area of interest.

Additional analysis was conducted to investigate the model sensitivity to the four selected parameters under different storm conditions. Parameters relevant to wave dissipation ($alpha$, $gamma$, and $gamma2$) were largely affected by the variation in $facua$ (i.e., relatively insensitive compared to $facua$), and the relative insensitivity led to similar model performance from all different combinations of the three parameters. Therefore, the model sensitivity to each storm event under the four parameter combinations was consistent with that influenced only by $facua$. Consequently, the calibrated values of the three parameters tended to change to compensate for over- or underestimation of erosion volume when calibrated with $facua$, and the most reliable results were mainly obtained at $facua$ of 0.15 for both single and clustered storm conditions in this study site.

Finally, the predicted profile changes with a single parameter set for each storm case were compared with the observed values. The parameter set was composed of a *facua* of 0.15, with the remaining parameters as default ($\alpha = 1$, $\gamma = 0.52$, and $\gamma_2 = 0.3$), owing to the comparative insensitivity of the rest. The area model with the chosen parameter set captured equilibrium profile response well, despite poor performance on accretion profiles because sediment transport toward the above MSL was limited in the phase-averaged wave mode [53]. Other studies [54–56] have also pointed out the underestimation of run-up prediction in XBSB owing to the absence of short wave motions in the mode. To solve the problem in XBSB, Pender and Karunarathna (2013) [17] used particular parameter sets for accretive conditions as opposed to erosive conditions. Kombiadou et al., 2021 [19] applied the correction of run-up height and adjustment of the swash zone slope to predict accretion profiles. These results imply that XBSB requires different calibrations and corrections to model the accretion process by complementing the limitations of the surfbeat mode.

Contribution Points:

1. The cumulative storm power and resultant erosion volume closely correlated with the overall model sensitivity compared to other features in the datasets (e.g., wave directions, pre-storm beach state, and the time interval between bathymetric surveys) at the study site. This result may help modelers decide which factors preferentially have to be considered in calibration in the area model under complex bathymetry.
2. The analysis of model sensitivity to different storm events guides the selection of event-specific data for model calibration.
3. XBSB can simulate the equilibrium profile response with reduced uncertainty and equifinality induced by the trial of various parameter combinations.
4. This study highlights the effect of event-specific calibration of a process-based model in realizing better prediction and forecasting of coastal erosion, thereby resulting in more effective hazard mitigation. Therefore, the results of this study will benefit not only researchers but also government agencies involved in disaster management.

Author Contributions: Conceptualization, H.J. and K.D.; methodology, H.J. and K.D.; software, H.J.; validation, H.J.; formal analysis, H.J.; investigation, H.J. and K.D.; resources, I.K. and S.C.; data curation, I.K. and S.C.; writing—original draft preparation, H.J. and K.D.; writing—review and editing, H.J., K.D., I.K. and S.C.; visualization, H.J.; supervision, K.D. and I.K.; project administration, K.D.; funding acquisition, K.D. and I.K. All authors have read and agreed to the published version of the manuscript.

Funding: This research was partly supported by the National Research Foundation of Korea (NRF-2022R111A3065599) and the project titled ‘Establishment of the Ocean Research Station in the Jurisdiction Zone and Convergence Research’, funded by the Ministry of Oceans and Fisheries.

Institutional Review Board Statement: Not applicable.

Informed Consent Statement: Not applicable.

Data Availability Statement: Not applicable.

Conflicts of Interest: The authors declare no conflict of interest.

References

1. Vousdoukas, M.I.; Ranasinghe, R.; Mentaschi, L.; Plomaritis, T.A.; Athanasiou, P.; Luijendijk, A.; Feyen, L. Sandy coastlines under threat of erosion. *Nat. Clim. Chang.* **2020**, *10*, 260–263. [[CrossRef](#)]
2. Matheen, N.; Harley, M.D.; Turner, I.L.; Splinter, K.D.; Thran, M.C.; Simmons, J.A. Bathymetric Data Requirements for Operational Coastal Erosion Forecasting Using XBeach. *J. Mar. Sci. Eng.* **2021**, *9*, 1053. [[CrossRef](#)]
3. Kobayashi, N.; Farhadzadeh, A.; Melby, J.; Johnson, B.; Gravens, M. Wave overtopping of levees and overwash of dunes. *J. Coast. Res.* **2010**, *2010*, 888–900. [[CrossRef](#)]
4. Larson, M.; Kraus, N.C. *SBEACH: Numerical Model for Simulating Storm-Induced Beach Change*; Report 1, Empirical Foundation and Model Development ; Technical Report CERC-89-9; U.S Army Engineer Waterways Experiment Station, Coastal Engineering Research Center: Washington, DC, USA, 1989.

5. Roelvink, D.; Reniers, A.; van Dongeren, A.; van Thiel de Vries, J.; McCall, R.; Lescinski, J. Modelling storm impacts on beaches, dunes and barrier islands. *Coast. Eng.* **2009**, *56*, 1133–1152. [[CrossRef](#)]
6. Simmons, J.A.; Harley, M.D.; Marshall, L.A.; Turner, I.L.; Splinter, K.D.; Cox, R.J. Calibrating and assessing uncertainty in coastal numerical models. *Coast. Eng.* **2017**, *125*, 28–41. [[CrossRef](#)]
7. Simmons, J.A.; Splinter, K.D.; Harley, M.D.; Turner, I.L. Calibration data requirements for modelling subaerial beach storm erosion. *Coast. Eng.* **2019**, *152*, 103507. [[CrossRef](#)]
8. Elsayed, S.M.; Oumeraci, H. Effect of beach slope and grain-stabilization on coastal sediment transport: An attempt to overcome the erosion overestimation by XBeach. *Coast. Eng.* **2017**, *121*, 179–196. [[CrossRef](#)]
9. Van Enckevort, I.M.J.; Ruessink, B.G.; Coco, G.; Suzuki, K.; Turner, I.L.; Plant, N.G.; Holman, R.A. Observations of nearshore crescentic sandbars. *J. Geophys. Res. Ocean.* **2004**, *109*, 1–17. [[CrossRef](#)]
10. Castelle, B.; Ruessink, B.G.; Bonneton, P.; Marieu, V.; Bruneau, N.; Price, T.D. Coupling mechanisms in double sandbar systems. Part 1: Patterns and physical explanation. *Earth Surf. Process. Landf.* **2010**, *35*, 476–486. [[CrossRef](#)]
11. Orzech, M.D.; Reniers, A.J.H.M.; Thornton, E.B.; MacMahan, J.H. Megacusps on rip channel bathymetry: Observations and modeling. *Coast. Eng.* **2011**, *58*, 890–907. [[CrossRef](#)]
12. Price, T.D.; Ruessink, B.G.; Castelle, B. Morphological coupling in multiple sandbar systems—A review. *Earth Surf. Dyn.* **2014**, *2*, 309–321. [[CrossRef](#)]
13. Ranasinghe, R.; Turner, I.L. Shoreline response to submerged structures: A review. *Coast. Eng.* **2006**, *53*, 65–79. [[CrossRef](#)]
14. Nordstrom, K.F. Living with shore protection structures: A review. *Estuar. Coast. Shelf Sci.* **2014**, *150*, 11–23. [[CrossRef](#)]
15. Bolle, A.; Mercelis, P.; Roelvink, D.; Haerens, P.; Trouw, K. Application and Validation of Xbeach for Three Different Field Sites. *Coast. Eng. Proc.* **2011**, *1*, 40. [[CrossRef](#)]
16. Simmons, J.A. Improved Model Calibration Techniques for Predicting Coastal Storm Erosion. Ph.D. Thesis, The University of New South Wales, Sydney, Australia, March 2018.
17. Pender, D.; Karunarathna, H. A statistical-process based approach for modelling beach profile variability. *Coast. Eng.* **2013**, *81*, 19–29. [[CrossRef](#)]
18. Kalligeris, N.; Smit, P.; Ludka, B.C.; Guza, R.T.; Gallien, T.W. Calibration and assessment of process-based numerical models for beach profile evolution in southern California. *Coast. Eng.* **2020**, *158*, 103650. [[CrossRef](#)]
19. Kombiadou, K.; Costas, S.; Roelvink, D. Simulating destructive and constructive morphodynamic processes in steep beaches. *J. Mar. Sci. Eng.* **2021**, *9*, 86. [[CrossRef](#)]
20. Rafati, Y.; Hsu, T.J.; Elgar, S.; Raubenheimer, B.; Quataert, E.; van Dongeren, A. Modeling the hydrodynamics and morphodynamics of sandbar migration events. *Coast. Eng.* **2021**, *166*, 103885. [[CrossRef](#)]
21. Karunarathna, H.; Pender, D.; Ranasinghe, R.; Short, A.D.; Reeve, D.E. The effects of storm clustering on beach profile variability. *Mar. Geol.* **2014**, *348*, 103–112. [[CrossRef](#)]
22. Dissanayake, P.; Brown, J.; Wisse, P.; Karunarathna, H. Effects of storm clustering on beach/dune evolution. *Mar. Geol.* **2015**, *370*, 63–75. [[CrossRef](#)]
23. Callaghan, D.P.; Ranasinghe, R.; Roelvink, D. Probabilistic estimation of storm erosion using analytical, semi-empirical, and process based storm erosion models. *Coast. Eng.* **2013**, *82*, 64–75. [[CrossRef](#)]
24. De Boer, W.; Huisman, B.; Yoo, J.; McCall, R.; Scheel, F.; Swinkels, C.M.; Friedman, J.; Luijendijk, A.; Walstra, D. Understanding coastal erosion processes at the Korean east coast. In Proceedings of the Coastal Dynamics 2017, Helsingør, Denmark, 12–16 June 2017; pp. 1336–1347. Available online: https://pure.tudelft.nl/ws/files/31196730/014_DeBoer_Wiebe.pdf (accessed on 11 August 2022).
25. Jin, H.; Do, K.; Chang, S.; Kim, I.H. Field Observation of Morphological Response to Storm Waves and Sensitivity Analysis of XBeach Model at Beach and Crescentic Bar. *J. Korean Soc. Coast. Ocean Eng.* **2020**, *32*, 446–457. [[CrossRef](#)]
26. Van Rijn, L.C.; Waslra, D.J.R.; Grasmeyer, B.; Sutherland, J.; Pan, S.; Sierra, J.P. The predictability of cross-shore bed evolution of sandy beaches at the time scale of storms and seasons using process-based profile models. *Coast. Eng.* **2003**, *47*, 295–327. [[CrossRef](#)]
27. Wright, L.D.; Short, A.D. Morphodynamic variability of surf zones and beaches: A synthesis. *Mar. Geol.* **1984**, *56*, 93–118. [[CrossRef](#)]
28. Cho, Y.J.; Kim, I.H. Preliminary Study on the Development of a Platform for the Selection of Optimal Beach Stabilization Measures against the Beach Erosion—Centering on the Yearly Sediment Budget of Mang-Bang Beach. *J. Korean Soc. Coast. Ocean Eng.* **2019**, *31*, 28–39. [[CrossRef](#)]
29. Oh, S.-H.; Jeong, W.-M.; Lee, D.-Y.; Kim, S. Analysis of the Reason for Occurrence of Large-Height Swell-like Waves in the East Coast of Korea Analysis of the Reason for Occurrence of Large-Height Swell-like Waves in the East Coast of Korea. *J. Korean Soc. Coast. Ocean Eng.* **2010**, *22*, 101–111.
30. Castelle, B.; Marieu, V.; Bujan, S.; Splinter, K.D.; Robinet, A.; Sénéchal, N.; Ferreira, S. Impact of the winter 2013–2014 series of severe Western Europe storms on a double-barred sandy coast: Beach and dune erosion and megacusp embayments. *Geomorphology* **2015**, *238*, 135–148. [[CrossRef](#)]
31. Dissanayake, P.; Brown, J.; Karunarathna, H. Impacts of storm chronology on the morphological changes of the Formby beach and dune system, UK. *Nat. Hazards Earth Syst. Sci.* **2015**, *15*, 1533–1543. [[CrossRef](#)]

32. Wright, L.D.; Short, A.D.; Green, M.O. Short-term changes in the morphodynamic states of beaches and surf zones: An empirical predictive model. *Mar. Geol.* **1985**, *62*, 339–364. [[CrossRef](#)]
33. Yates, M.L.; Guza, R.T.; O'Reilly, W.C.; Hansen, J.E.; Barnard, P.L. Equilibrium shoreline response of a high wave energy beach. *J. Geophys. Res. Ocean.* **2011**, *116*, 1–13. [[CrossRef](#)]
34. Ludka, B.C.; Guza, R.T.; O'Reilly, W.C.; Yates, M.L. Field evidence of beach profile evolution toward equilibrium. *J. Geophys. Res. Ocean.* **2015**, *120*, 7574–7597. [[CrossRef](#)]
35. Athanasiou, P. Understanding the Interactions between Crescentic Bars, Human Interventions and Coastline Dynamics at the East Coast of South Korea. Master's Thesis, Delft University of Technology, Delft, The Netherlands, 19 September 2017.
36. Cohn, N.; Ruggiero, P.; Ortiz, J.; Walstra, D.J. Investigating the role of complex sandbar morphology on nearshore hydrodynamics. *J. Coast. Res.* **2014**, *70*, 53–58. [[CrossRef](#)]
37. Do, K.; Yoo, J. Morphological response to storms in an embayed beach having limited sediment thickness. *Estuar. Coast. Shelf Sci.* **2020**, *234*, 106636. [[CrossRef](#)]
38. Passeri, D.L.; Long, J.W.; Plant, N.G.; Bilskie, M.V.; Hagen, S.C. The influence of bed friction variability due to land cover on storm-driven barrier island morphodynamics. *Coast. Eng.* **2018**, *132*, 82–94. [[CrossRef](#)]
39. Roelvink, D.; Costas, S. Beach berms as an essential link between subaqueous and subaerial beach/dune profiles. *Geo-Temas* **2017**, *17*, 79–82.
40. Van der Lugt, M.A.; Quataert, E.; van Dongeren, A.; van Ormondt, M.; Sherwood, C.R. Morphodynamic modeling of the response of two barrier islands to Atlantic hurricane forcing. *Estuar. Coast. Shelf Sci.* **2019**, *229*, 106404. [[CrossRef](#)]
41. Fang, K.; Wang, H.; Sun, J.; Zhang, J.; Liu, Z. Including Wave Diffraction in XBeach: Model Extension and Validation. *J. Coast. Res.* **2020**, *36*, 116. [[CrossRef](#)]
42. Daly, C.; Roelvink, D.; van Dongeren, A.; van Thiel de Vries, J.; McCall, R. Validation of an advective-deterministic approach to short wave breaking in a surf-beat model. *Coast. Eng.* **2012**, *60*, 69–83. [[CrossRef](#)]
43. Cho, M.; Yoon, H.D.; Do, K.; Kim, I. Calibration and Assessment of Bed Evolution Model in an Embayed Beach with Submerged Breakwaters. *J. Coast. Res.* **2021**, *114*, 514–518. [[CrossRef](#)]
44. Nederhoff, C.M. (Kees) Modelling the Effects of Hard Structures on Dune Erosion and Overwash. Hindcasting the Impact of Hurricane Sandy on New Jersey with XBeach. Master's Thesis, Delft University of Technology, Delft, The Netherlands, 14 November 2014.
45. De Vet, P.L.M.; McCall, R.T.; Den Bien, J.P.; Stive, M.J.F.; Van Ormondt, M. Modelling Dune Erosion, Overwash and Breaching at Fire Island (Ny) during Hurricane Sandy. In Proceedings of the Coastal Sediment 2015, San Diego, CA, USA, 11–15 May 2015; pp. 1–10.
46. Roelvink, J.A. Dissipation in random wave groups incident on a beach. *Coast. Eng.* **1993**, *19*, 127–150. [[CrossRef](#)]
47. Daly, C.; Roelvink, D.; Van Dongeren, A.; Van Thiel de Vries, J.; McCall, R. Short Wave Breaking Effects on Low Frequency Waves. *Coast. Eng. Proc.* **2011**, *1*, 20. [[CrossRef](#)]
48. Roelvink, D.; McCall, R.; Mehvar, S.; Nederhoff, K.; Dastgheib, A. Improving predictions of swash dynamics in XBeach: The role of groupiness and incident-band runup. *Coast. Eng.* **2018**, *134*, 103–123. [[CrossRef](#)]
49. Van Thiel de Vries, J. Dune erosion above revetments. In Proceedings of the 33rd International Conference on Coastal Engineering, Santander, Spain, 1–6 July 2012; pp. 1–13.
50. Bae, H.; Do, K.; Kim, I.H.; Chang, S. Proposal of parameter range that offered optimal performance in the coastal morphodynamic model (XBeach) through GLUE. *J. Ocean Eng. Technol.* **2022**, *36*, 251–269. [[CrossRef](#)]
51. Soulsby, R.L. *Dynamics of Marine Sands*; Thomas Telford Publications: London, UK, 1997.
52. Hornberger, G.M.; Spear, R.C. An approach to the preliminary analysis of environmental systems. *J. Environ. Manag.* **1981**, *12*, 7–18.
53. Daly, C.; Floc'h, F.; Almeida, L.P.; Almar, R. Modelling accretion at nha trang beach, vietnam. In Proceedings of the International Conference on Coastal Dynamics, Helsingor, Denmark, 12–16 June 2017; pp. 1886–1896.
54. Stockdon, H.F.; Thompson, D.M.; Plant, N.G.; Long, J.W. Evaluation of wave runup predictions from numerical and parametric models. *Coast. Eng.* **2014**, *92*, 1–11. [[CrossRef](#)]
55. Palmsten, M.L.; Splinter, K.D. Observations and simulations of wave runup during a laboratory dune erosion experiment. *Coast. Eng.* **2016**, *115*, 58–66. [[CrossRef](#)]
56. De Beer, A.F.; McCall, R.T.; Long, J.W.; Tissier, M.F.S.; Reniers, A.J.H.M. Simulating wave runup on an intermediate-reflective beach using a wave-resolving and a wave-averaged version of XBeach. *Coast. Eng.* **2021**, *163*, 103788. [[CrossRef](#)]